New Journal of Glass and Ceramics, 2014, 4, 19-28
Published Online April 2014 in SciRes. http://www.scirp.org/journal/njgc
http://dx.doi.org/10.4236/njgc.2014.42003

Scientific Research

Structural, Magnetic and Dielectric Properties of Fe-Co Co-Doped $Ba_{0.9}Sr_{0.1}TiO_3$ Prepared by Sol Gel Technique

Inas Kamal Batttisha[1*], Ibrahim Sayed Ahmed Farag[1], Mostafa Kamal[2], Mohamed Ali Ahmed[3], Emad Girgis[1], Hesham Azmi El Meleegi[4], Fawzi Gooda El Desouky[1]

[1]National Research Center (NRC), Solid State Physics Department, Dokki, Giza, Egypt
[2]Metal Physics Laboratory, Physics Department, Faculty of Science, Mansoura University, Mansoura, Egypt
[3]Materials Science Lab (1), Physics Department, Faculty of Science, Cairo University, Giza, Egypt
[4]National Research Centre (NRC), Thin Film Lab, Electron Microscope Department, Dokki, Giza, Egypt
Email: [*]szbasha@yahoo.com, [*]ibattisha@gmail.com

Received 17 January 2014; revised 17 February 2014; accepted 2 March 2014

Abstract

The structural, dielectric and magnetic properties of pure and Fe-Co co-doped $Ba_{0.9}Sr_{0.1}TiO_3$, ($Ba_{(1-x)}Sr_xTiO_3$, where (x = 0.10) and ($Ba_{0.9}Sr_{0.1}Ti_{(1-x-y)}Fe_xCo_yO_3$), where ($x$ = 0.1, y = 0) and (x = 0 and y = 0.10) and (x = 0.5, y = 0.5) in powder form, abbreviated as (BST) and (BST10FO), (BST10CO) and (BST5F5CO), respectively were prepared by a modified sol gel technique. Crystallization, surface morphology and electrical behavior of BST are improved by Fe^{3+} and Co^{2+} ions with optimized grain size. Phase identification by using X-ray diffraction and surface morphology will be studied by using transmission electron microscope (TEM) and scanning electron microscope imaging (SEM). Phase identification by using X-ray diffraction and surface morphology evaluation by using transmission electron microscope (TEM) and scanning electron microscope imaging (SEM) will be studied. The nano-scale presence and the formation of the tetragonal perovskite phase as well as the crystallinity were detected using the mentioned techniques. The dielectric properties of the prepared samples have been investigated as a function of temperature and frequency. The dielectric measurements are carried out in the frequency range of 42 Hz - 1 MHz, at temperature ranging between 25˚C and 250˚C. The results showed an abrupt decrease in the dielectric permittivity by increasing the frequency range. The magnetic hysteresis loop confirmed enhancement in the magnetization properties by co-doping with Fe^{3+}-Co^{2+} ions. An increase in the saturation of the magnetization at room temperature was detected by decreasing the crystallite sizes of the prepared samples.

[*]Corresponding author.

How to cite this paper: Batttisha, I.K., *et al.* (2014) Structural, Magnetic and Dielectric Properties of Fe-Co Co-Doped $Ba_{0.9}Sr_{0.1}TiO_3$ Prepared by Sol Gel Technique. *New Journal of Glass and Ceramics*, **4**, 19-28.
http://dx.doi.org/10.4236/njgc.2014.42003

Keywords

Sol Gel, Nano-Structure, Magnetic Hysteresis Loop, Dielectric Permittivity, Nano-Composite $BaSrTiO_3$ (BST), TEM, XRD, SEM

1. Introduction

Complex oxides are very appealing materials from a function point of view, due to their wide range of properties: such as ferroelectricity, ferromagnetism, ferroelasticity etc. They can be metals, insulator, semiconductors, superconductor etc. The coupling between some of these properties can give rise to new applications. Some of these oxides have the unique properties of both ferromagnetism and ferroelectricity in a single phase. This opens broader applications in transducers, magnetic field sensors and information storage industry and multifunctional devices such as memory devices [1]-[4]. The relationship between multiferroic and magnetoelectric materials is well reflected by **Figure 1** [5].

A single phase multiferroic material is the one that possesses two of the three "ferroic" properties *i.e*. ferroelectricity, ferromagnetism and ferroelasticity. Generally current trend is to exclude the requirement for ferroelastic property. Magnetoelectric coupling describes the coupling between magnetic and electric order parameters [6]-[10].

This paper aims to study the structural, dielectric and magnetic properties of pure BST and (Fe and Co) co-doping into ferroelectrics BST. The structure and phase identification will be evaluated by XRD. The TEM and SEM of pure barium strontium titinate (B10ST), B10ST10C and B10ST5C5F revealed the presence of the nano-phase in the prepared samples. BST ceramics exhibit excellent single tetragonal phase by using sol gel technique as preparation process. A large amount of doping of Fe-Co which mainly acts as an acceptor to replace Ti in the B-site, leads to the appearance of lattice defects and vacancies. The dielectric properties of the samples will be studied in frequency range of 42 Hz up to 1 MHz. Ferroelectricity and ferromagnetism of samples are simultaneously observed. The magnetic measurements were carried out at room temperature using lakeshore vibrating sample magnetometer (VSM 7410) model lakeshore 7110.

2. Materials and Methods

2.1. Samples Preparation

$Ba_{0.9}Sr_{0.1}TiO_3$, (BST) and $Ba_{0.9}Sr_{0.1}Ti_{(1-x-y)}Fe_xCo_yO_3$, where ($x$ = 0.1, y = 0) (BST10F), (x = 0, y = 0.10), (BST10C) and (x = 0.5, y = 0.5), (BST5F5C), respectively in powder forms were prepared by a modified sol gel method. **Table 1** shows dopant concentration, sample abbreviation, chemical formula and oxygen vacancies of Fe^{3+} and Co^{2+} ions concentration doped nano-composite B10ST powders.

The mentioned samples have been prepared using barium acetate ($Ba(Ac)_2$) (99%, Sisco Research Labo- ratories PVT.LTD, India) and titanium butoxide ($Ti(C_4H_9O)_4$), (97%, Sigma-Aldrich, Germany) are used as the starting materials; acetyl acetone (AcAc, $C_5H_8O_2$), (98%, Fluka, Switzerland) acetic acid (HAc)-H_2O mixture (96%, Adwic, Egypt) were adopted as solvents of ($Ti(C_4H_9O)_4$), and $Ba(Ac)_2$, respectively. Strontium bromide is

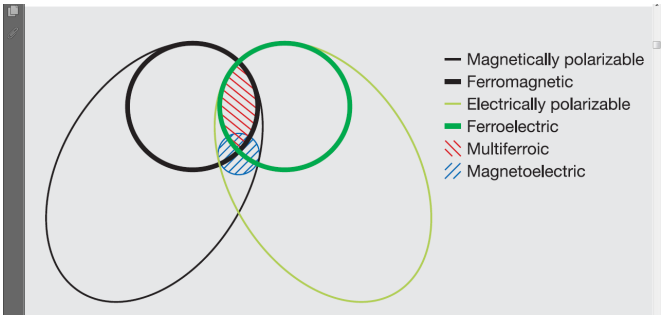

Figure 1. The relationship between multiferroic and magnetoelectric materials [5].

Table 1. Dopant concentration, sample abbreviation, chemical formula and oxygen vacancies of Fe^{3+} and Co^{2+} ions concentration doped nano-composite B10ST powders.

Dopant Concentration	Sample abbreviations	Chemical Formula	δ
$x = 0.1, y = 0, z = 0$	B10ST	$Ba_{0.9}Sr_{0.1}Ti_1O_3$	$\delta = 0.000$
$x = 0.1, y = 0.1, z = 0$	B10ST10F	$Ba_{0.9}Sr_{0.1}Ti_{0.9}Fe_{0.1}O_{2.95}$	$\delta = 0.050$
$x = 0, y = 0, z = 0.1$	B10ST10C	$Ba_{0.9}\ Sr_{0.1}Ti_{0.9}\ Co_{0.1}O_{2.9}$	$\delta = 0.100$
$x = 0.1, y = 0.05, z = 0.05$	B10ST5F5C	$Ba_{0.9}Sr_{0.1}Ti_{0.9}Fe_{0.05}Co_{0.05}O_{2.925}$	$\delta = 0.075$

added to the precursor with constant 0.1 mol % molar ratios. Iron and cobalt nitrates are added to the final solution and its content has been changed. Densification of the gel is achieved by sintering in air for one hour at heat treatment temperature 750˚C, in a muffle furnace type (Carbolite CWF 1200).

2.2. Characterization

The phases of the obtained samples are characterized by X-ray diffraction (XRD) (BRUKUR D8 ADVANCED TARGET Cu Kα with Secondary monochromatic KV = 40, mA = 40 Germany) in a wide range of Bragg angle from 10˚ - 80˚ using Cu Ka (1.5406 Å) radiation with a step size of 0.02 at room temperature. The crystallite size (G) is determined from the Scherrer's equation;

$$G = K\lambda / D\cos\theta \tag{1}$$

where K is the Scherer constant, in the present case K = (0.9), λ is the wavelength and D is the full width (in radians) of the peak at half maximum (FWHM) intensity. The microstructure and surface morphology of the samples were observed by (TEM) transmission electron microscope (using JEOL JEM-1230 equipment operat- ing at 120 kV with attached CCD camera) and (SEM) scanning electron microscope (Quanta 250 FEG (Field emission Gun) was used to determine grain size and uniformity of the sample analysis. The phase transitions above room temperature have been investigated by DTA (SDT Q 600 V 20.9 Build 20) measurements.

Magnetization hysteresis (M-H) measurements were carried out at room temperature using lakeshore vibrating sample magnetometer (VSM 7410) model lakeshore 7110.

The relative dielectric permittivity was calculated using the relations:

$$\varepsilon' = Cd / \varepsilon_o A \tag{1}$$

where C is the capacitance of the measured sample in Farad, d is the thickness of the sample in meters, A is the cross section area of the sample and ε_o is the permittivity of free space (8.854×10^{-12} Fm^{-1}).

$$\varepsilon'' = \varepsilon' \times \tan\delta \tag{2}$$

where, ε'' is the dielectric loss and $\tan\delta$ is the loss tangent.

3. Results and Discussion

3.1. XRD Investigation

For comparison between the un-doped and co-doped samples with Fe^{3+} and Co^{2+} ions calcinated at constant temperature 850˚C for four hours, the XRD patterns of pure B10ST (a) and the doped powder samples with (10 mol% Fe^{3+}) (B10ST10F) (b), (10 mol% Co^{2+}) (B10ST10C) (c) and doped with both (Fe^{3+} & Co^{2+} at 5 mol%) (B10ST5F5C) (d) were plotted in **Figure 2** (a)-(d), respectively. All the diffraction peaks are indexed and the tetragonal structure phase is identified [11]. The XRD patterns of the prepared samples are in good agreement with the tetragonal BST phase (ICCD card number 44-0093,) as shown in **Figure 2** (b)-(d). Very weak line corresponding to the residual carbonates phases, such as $BaCO_3$, $SrCO_3$ and (Ba, Sr) CO_3 were appeared in the doped samples with no other observable iron and cobalt oxide phases in the systems [12] [13]. So the Fe^{3+} and Co^{2+} ions are embedded in the BST crystal lattice and substitute the Ti^{4+} ions where no obvious secondary phase from Fe^{3+}, Co^{2+} and Ti^{4+} ions are observed in the diffraction patterns as shown in **Figure 2** (b)-(d).

From the **Table 2** we can see that the lattice parameters of the B10ST and B10ST10F samples exhibit a slight variation, but the crystal structures remain almost the same. The values of lattice parameter (a) and (c) increase

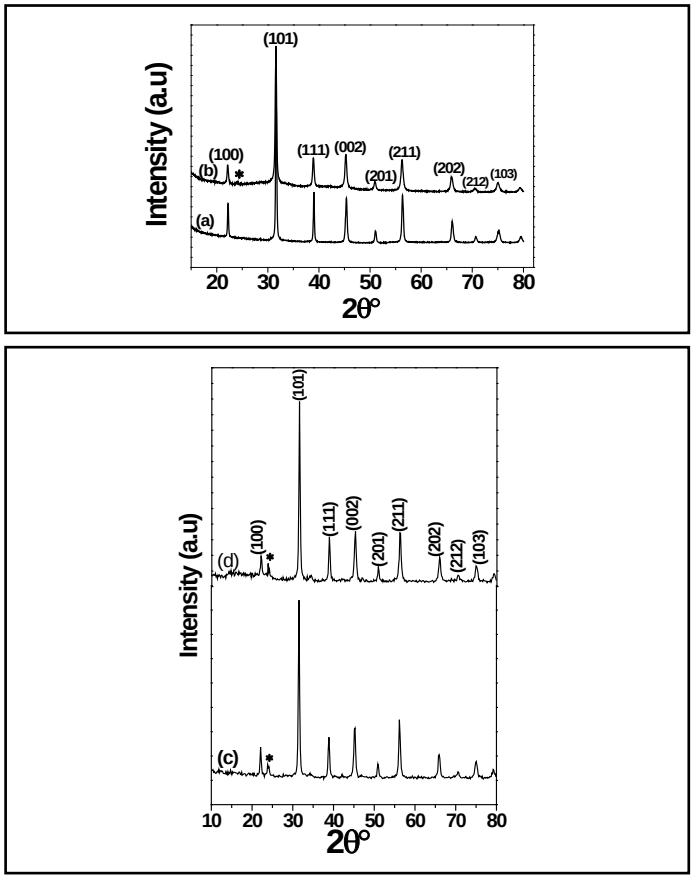

Figure 2. XRD patterns of (B10ST) (a), (B10ST10F) (b), (B10ST10C) (c) and (B10ST5F5CO) (d) in powder form calcinated at 850˚C for 4 h (Ba, $Sr(Co_3)$ is marked by *).

by doping with the Fe^{3+} ions, indicating a lattice expansion of BSTF systems. For instance, the unit cell volume increases due to the different sizes between Fe^{3+} and Ti^{4+} ions (0.645 Å for Fe^{3+} and 0.68 Å for Ti^{4+}) [13] and the possible ion vacancies presented in the lattices as shown in **Table 1**. In the sample doped with cobalt oxide some Co^{2+} cation proportions exist and this cation can be considered as acceptor dopants as it has a lower valence than Ti^{4+}. The substitution of Ti^{4+} by Co^{2+} would give rise vacancy in the oxygen sub-lattice as in **Figure 2** (c). The lattice parameter of the doped samples is carefully determined, as listed in **Table 1**. The values of lattice parameter (a) and (c) is increased by doping with the Co^{2+} ions, indicating a lattice expansion of B10ST10C system. The unit cell volume increases as shown in **Table 1** which can be attributed to the different sizes between Co^{2+} and Ti^{4+} ions (0.65 Å for Co^{2+} and 0.68 Å for Ti^{4+}). These vacancies may be favorable for stabilizing the tetragonal structure of BSTC systems.

The average crystallite sizes of our samples calculated using Scherrer's formula were decreased by doping with both Fe^{3+} and Co^{2+} ions to be equal to 52, 31, 31.3, 27.45 for B10ST, (B10ST10F), (B10ST10C) and (B10ST5F5C), respectively as detected in **Table 1**.

3.2. Transmission Electron Microscope (TEM) Study

Figure 3 shows the representative TEM of B10ST5F5C ≈ (27 nm), thermally synthesized in air for 4 h at 850˚C. Some degree of agglomerates has been found in the clusters consisting of many small particles. The calculated average particle size from TEM was about 27 nm for B10ST5F5C, which is nearly agree with the value obtained from XRD for the same sample 27.45 nm. The TEM was used to confirm the data calculated from XRD patterns and that the sample is in nano-scale. Images in **Figure 3**, clearly shows that the additive of cobalt and iron oxides have leads to a grains refining [14] [15].

Table 2. Lattice parameters and unit cell volume of B10ST, B10STF, B10ST10C and B10ST5F5C.

Sample abbreviations	Crystal size (XRD) nm	a, b (Å)	c (Å)	c/a	V (Å)^3
B10ST	52.00	3.9996	3.9995	0.9999	63.97879
B10ST10F	31.00	4.0066	3.9980	0.99875	64.17926
B10ST10C	31.30	4.00725	4.00194587	0.9986	64.26316
B10ST5F5C	27.45	4.00139	4.001985	1.00015	64.07627

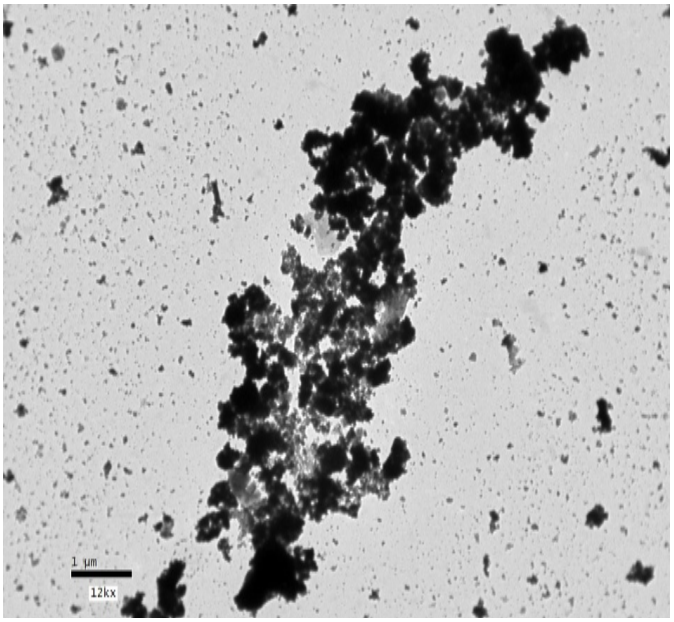

Figure 3. The TEM micrograph of (B10ST5F5C) powder sample calcinated at 850˚C for 4 h.

3.3. Scanning Electron Microscope (SEM) Study

Figure 4, shows the surface morphologies obtained through Scanning Electron Microscope (SEM) with different magnifications for nanostructure pure (B10ST) and co-doped with both Fe^{3+} and Co^{2+} ions (B10ST10F) (B10ST10C) and (B10ST5F5C) powder samples calcined for 4 hours at 850˚C are illustrated in **Figures 4(a)-(e)**, respectively. These images show grains typical of pure B10ST powders, which consist of a granular microstructure with irregular shaped grains, with two different magnifications and in two different areas, as shown in **Figure 4(a)** and **Figure 4(b)**. The images in **Figures 4(c)-(e)** show comparatively more accumulated particles with higher density showing an increase in grain growth by doping with both Fe^{3+} and Co^{2+} ions and the particles have a well-defined shape.

Fe^{3+} and Co^{2+} dopant contents are effective to increase the density and improve the microstructure homogeneity of the prepared powder samples. The particles are nearly tetragonal in nature and less agglomerated in the pure B10ST sample and indicate the well-distributed crystallites and the dense nanoparticles surfaces. While by doping with Fe^{3+} and Co^{2+} the particles have a well-defined shape, and they are still tetragonal and highly dispersed. This is might be due to some aggregates of particles together.

3.4. Dielectric Properties of B10ST, B10ST10F, B10ST10C and B10ST5F5C, Respectively

Figure 5 shows the variation of dielectric constant, (ε') measured at room temperature as a function of frequency (f) in the frequency range (10 KHz - 5 MHz) for pure B10ST powder sample and doped samples B10ST10F, B10ST10C and B10ST5F5C, respectively. We can see a sharp fall in the value of (ε') for the pure BS10T nanoparticles that is followed by a rise in the (ε') value for B10ST10F and B10ST5F5C, respectively.

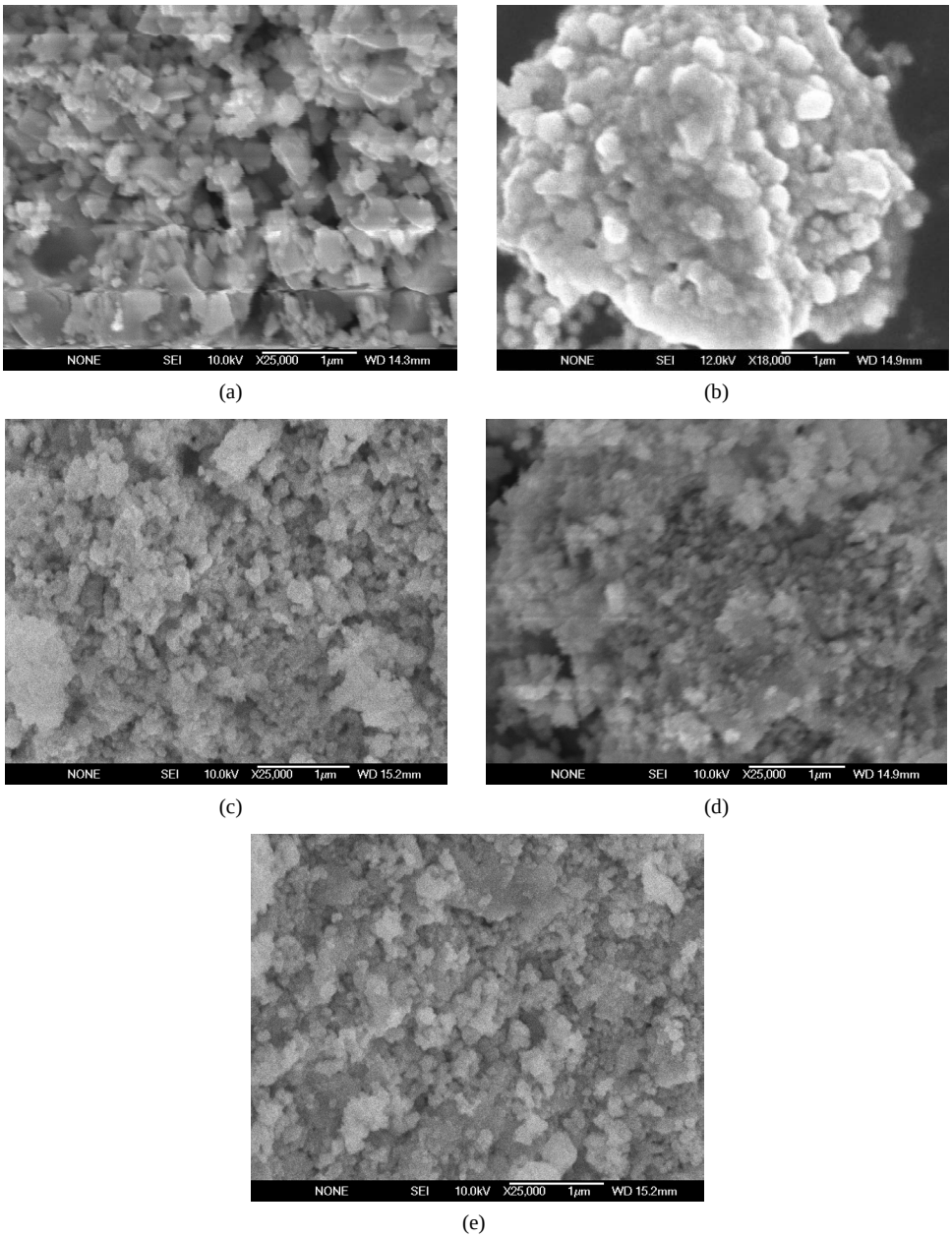

Figure 4. The SEM micrograph of pure (B10ST) (a) calcined at 750˚C for one hour [13], pure (B10ST) (b) calcined at 850˚C for 4 hours, (B10ST10C) (c), (B10ST10F) (d) and (B10ST5F5C) (e), all calcinated for 4 h at 850˚C.

It is evident that the dielectric constant (ε') decreases with increasing frequency and becomes nearly constant at the higher frequencies range. It follows the dipole relaxation where at low frequencies the dipoles follow the frequency of the applied field. The value of dielectric constant is highest for the B10ST10C. The decrease in (ε') value as a function of frequency is due to the electric dipole response in the prepared samples which, decreased at higher frequencies, where it need some time for realignment and cannot follow electric-field changes. Also the periodic reversal of the electric field occurred so fast that there was no excess charge carrier diffusion in the direction of the field. As the frequency increased, the dipoles were less able to rotate and maintain phase with the field. Thus, they reduced their contribution to the polarization field, and hence an observed reduction in the real part (ε') is appeared. Where the low frequency dispersion region is attributed to the charge accumulation at the electrode—sample interface.

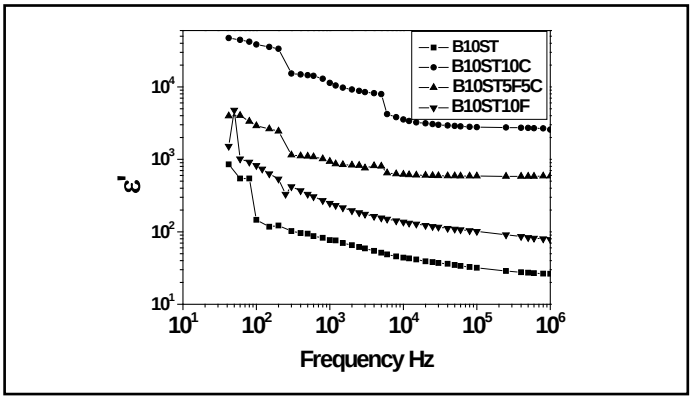

Figure 5. Relative permittivity (ε') of B10ST, and doped samples, B10ST10F, B10ST10C and B10ST5F5C, respectively.

For the dissipation factor $(\tan\delta)$ shown in **Figure 6**, it was noticed that this attenuation of $(\tan\delta)$ by increasing frequency might be attributed to the phonon dipole interaction which, led to a lowering of the energy transferred to the dielectric medium. Also, as the frequency increased, the dipoles polarization tended to zero and tan δ depended only on electronic polarization.

The low value of dissipation factor $(\tan\delta)$ indicated low conversion of electrical energy to heat energy and reduced power loss for the network. The dissipation factor, as well as other electrical parameters, depended on the frequency, humidity and purity of the sample.

The cationic size are (0.65 ˚A for Co^{2+}, 0.645 ˚A for $Fe^{3+}$and 0.68 ˚A for Ti^{4+}) Therefore, cationic substitution causes expansion in the ABO_3 structure, and modifies the dielectric properties as mentioned in the XRD section in this work. Addition of $Fe^{3+}$and Co^{2+} ions increases the relative permittivity of the ceramics compared to pure B10ST thermally treated at the same calcination temperature. These changes in electrical properties are believed to be associated with both improving microstructure and fired density [16] [17].

3.5. Magnetic Properties of B10ST10F and B10ST5F5C

Figure 7 shows the M-H curve of nano-structure B10ST, B10ST10F and B10ST5F5C, respectively. Measurement of magnetization in the nanocrystalline B10ST, with C.S. equal to (52 nm) sample was measured at room temperature and the results are as previously published by our team work [18] and as detected in **Table 3**. It is clear that a weak ferromagnetism at room temperature with a coercive field and saturation magnetization equal to 74.219000 Oe and 0.041556 emu/g, respectively, for pure B10ST was obtained. It may be mentioned that the 52 nm B10ST sample showed higher saturation magnetization. In contrast, the bulk B10ST sample failed to exhibit magnetic hysteresis, as expected it exhibits diamagnetic behavior at room temperature. It is therefore, understandable that an increase in the particle size eliminates the magnetism due to the decrease in the surface to volume ratio.

Both the B10ST10F and the B10ST5F5C samples exhibit ferromagnetism at room temperature with clear hysteresis loops. **Figure 7** shows M-H curves of B10ST10F and B10S5F5C respectively, in powder form calcined at 850˚C for 4 h. It is known that magnetism in oxide nanoparticles arises from vacancies. From **Table 3** we can see that oxygen vacancies for B10ST, B10ST10F and B10S5F5C increase by doping with different transition elements, respectively, as a result of different ionic radius, where Fe^{3+} and Co^{2+} ions mainly acts as an acceptor to replace Ti in the B-site, leading to the further ionization of Fe^{3+} and Co^{2} ions and the appearance of lattice defects and vacancies, which are favorable for single-phase. From Table 3 the saturated magnetization M_S increases by decreasing the B10ST, B10ST10F and B10S5F5C particle sizes, this result is in agreement with the previously reported [18]-[20], as the size of the grain decreases, the material reaches a single domain state where there is no domain wall and all the magnetic domains are completely separated from each other, the enhancement of magnetization also come from the magnetic moment per Fe^{3+} and Co^{2+} ions due to the combined contributions of magnetic Fe^{3+} and Co^{2+} ions distributed over pentahedral and octahedral Ti sites. The Co^{2+} ions presence led to the increase of anisotropy property, hence an increase in oxygen vacancies as a result of different size between Ti^{4+} and Co^{2+} was appeared.

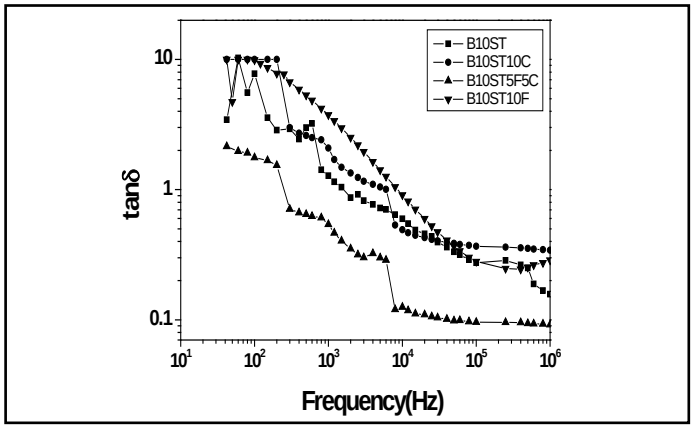

Figure 6. The dissipation factor (tan δ) of B10ST, and doped samples, B10ST10F, B10ST10C and B10ST5F5C, respectively.

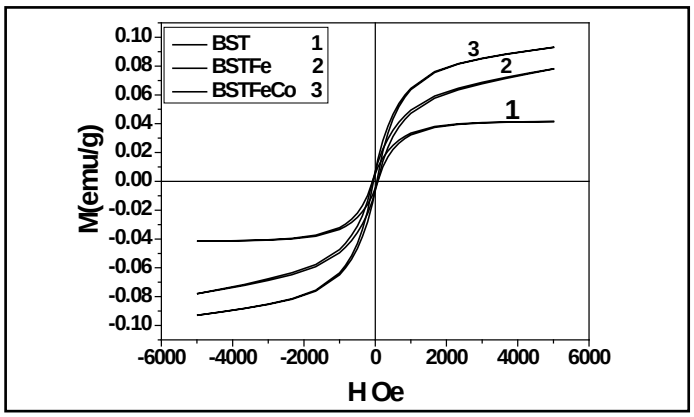

Figure 7. M-H curve of nano-structure (1) B10ST [18], (2) B10ST10F and (3) B10ST5F5C, respectively.

Table 3. Magnetic parameters at room temperature and particle size.

Samples	C.S nm	Hc (Coerc. Field)	Mr (Rem. Mag.)	Ms (Sat. Mag.)	Anisotropy
Abr.	Oe		emu/g	emu/g	Const.
B10ST	52.0	74.219	0.0049275	0.041556	1.5421
B10ST10F	31.00	72.196	0.0065871	0.07802	2.8163
B10ST5F5C	27.45	46.335	0.0059189	0.09298	2.15391

4. Conclusions

Nano-structure B10ST, B10ST10F, B10ST10C and B10S5F5C, have been successfully synthesized by a modified sol gel technique. XRD patterns confirm the tetragonal structure phase presence of the prepared samples. The prepared samples exhibit ferromagnetism at room temperature with clear hysteresis loops. It can be seen that the oxygen vacancies for B10ST , B10ST10F , B10ST10C and B10S5F5C increase respectively, as a result of different ionic radius, where Fe^{3+} and Co^{2+} ions, which mainly act as an acceptor to replace Ti in the B-site, leading to the further ionization of Fe^{3+} and Co^{2+} ions and the appearance of lattice defects and vacancies.

The results showed the achievement of Fe-doped BST with single phase perovskite structure and improved magnetic properties. The significant increase in magnetization by doping the BST with both Fe^{3+} and Co^{2+} ions increases the possibility of use for BST10F and BST5F5C in memory based applications.

Acknowledgements

The authors acknowledge 1) The team work of both projects—Imhotep project, 2009-2011, entitled; New nano-structured magnetoelectric materials based on doped BaTiO3: from ceramics to sol-gel deposited nano-films, for supporting—Imhotep project 2011-2013, entitled; Multiferroic nanostructure for multifunction sensors application, 2) Team work of Mena Sweden-Egyptian sharing project 2009-2015; entitled; Synthesis and investigation of the physical and electrical properties of BaSrTiO3 (BST) nano-structures prepared by sol-gel methods. For their support and helps in measuring all the Scanning Electron microscope of BST samples in this work.

References

[1] Li, B., Wanga, C., Liu, W., Ye, M. and Wang, N.G. (2013) Multiferroic Properties of La and Mn Co-Doped $BiFeO_3$ Nanofibers by Sol-Gel and Electrospinning Technique. *Materials Letters*, **90**, 45-48. http://dx.doi.org/10.1016/j.matlet.2012.09.012

[2] Bhushan, B., Das, D., Priyamc, A., Vasanthacharya, N.Y. and Kumar, S. (2012) Enhancing the Magnetic Characteristics of $BiFeO_3$ Nanoparticles by Ca,Ba Co-Doping Centre for Applied Physics. *Materials Chemistry and Physics*, **135**, 144-149. http://dx.doi.org/10.1016/j.matchemphys.2012.04.037

[3] Annapu Reddy, V., Patha, N.P. and Nath, R. (2012) Particle Size Dependent Magnetic Properties and Phase Transitions in Multiferroic $BiFeO_3$ Nano-Particles. *Journal of Alloys and Compounds*, **543**, 206-212. http://dx.doi.org/10.1016/j.jallcom.2012.07.098

[4] Wu, W.W., Cai, J.C., Wu, X.H., Liao, S. and Huang, A.G. (2012) $Co_{0.35}Mn_{0.65}Fe_2O_4$ Magnetic Particles: Preparation and Kinetics Research of Thermal Process of the Precursor. *Powder Technology*, **215-216**, 200-205. http://dx.doi.org/10.1016/j.powtec.2011.09.048

[5] Ahadi, K., Nemati, A., Mahdavi, S.M. and Vaezi, A. (2013) Effect of Simultaneous Chemical Substitution of A and B Sites on the Electronic Structure of $BiFeO_3$ Films Grown on $BaTiO_3/SiO_2/Si$ Substrate. *Journal of Materials Science*: *Materials in Electronics* **24**, 2128-2134. http://dx.doi.org/10.1007/s10854-013-1069-6

[6] Zhou, J., Wang, P., Qiu, Z., Zhu, G. and Liu, P. (2008) Flower-Like $Pb(Zr_{0.52}Ti_{0.48})O_3$ Nanoparticles on the $CoFe_2O_4$ Seeds. *Journal of Crystal Growth*, **310**, 508-512. http://dx.doi.org/10.1016/j.jcrysgro.2007.10.066

[7] Li, B., Wang, C., Liu, W., Zhong, Y. and An, R. (2012) Synthesis of Co-Doped Barium Strontium Titanate Nanofibers by Sol-Gel Electrospinning Process. *Materials Letters*, **75**, 207-210. http://dx.doi.org/10.1016/j.matlet.2012.02.035

[8] Bao, D. (2008) Multilayered Dielectric/Ferroelectric Thin Films and Superlattices. *Current Opinion in Solid State and Materials Science*, **12**, 55-61. http://dx.doi.org/10.1016/j.cossms.2009.01.006

[9] Gao, L., Zhai, J. and Yao, X. (2009) The Influence of Co Doping on the Dielectric, Ferroelectric and Ferromagnetic Properties of $Ba_{0.70}Sr_{0.30}TiO_3$ Thin Films. *Applied Surface Science*, **255**, 4521-4525. http://dx.doi.org/10.1016/j.apsusc.2008.11.064

[10] Solopan, S.A., Vyunov, O.I., Belous, A.G., Tovstolytkin, A.I. and Kovalenko, L.L. (2010) Magnetoelectric Effect in Composite Structures Based on Ferroelectric.Ferromagnetic Perovskites. *Journal of the European Ceramic Society*, **30**, 259-263. http://dx.doi.org/10.1016/j.jeurceramsoc.2009.05.043

[11] Deshpandea, S.B., Khollamb, Y.B., Bhoraskarb, S.V., Dateb, S.K., Sainkara, S.R. and Potdara, H.S. (2005) Synthesis and Characterization of Microwave-Hydrothermally Derived Ba1-xSrxTiO_3 Powders. *Materials Letters*, **59**, 293-296. http://dx.doi.org/10.1016/j.matlet.2004.10.006

[12] Zuo, X.H., Deng, X.Y., Chen, Y., Ruan, M., Li, W., Liu, B., Qu, Y. and Xu, B. (2010) A Novel Method for Preparation of Barium Strontium Titanate Nanopowders. *Materials Letters*, **64**, 1150-1153. http://dx.doi.org/10.1016/j.matlet.2010.02.034

[13] Mahani, R.M., Battisha, I.K., Salem, M.A. and Abou Hamad, A.B. (2010) Structure and Dielectric Behavior of Nano-Structure Ferroelectric $Ba_xSr_{1-x}TiO_3$ Prepared by Sol-Gel Method. *Journal of Alloys and Compounds*, **508**, 354-358. http://dx.doi.org/10.1016/j.jallcom.2010.05.060

[14] Wei, X., Xu, G., Ren, Z., Wang, Y., Shen, G. and Han, G. (2008) Size-Controlled Synthesis of $BaTiO_3$ Nanocrystals via a Hydrothermal Route. *Materials Letters*, **62**, 3666-3669. http://dx.doi.org/10.1016/j.matlet.2008.04.022

[15] El-Naggar, M.Y., Dayal, K., Goodwin, D.G. and Bhattacharya, K. (2006) Graded Ferroelectric Capacitors with Robust Temperature Characteristics. *Journal of Applied Physics*, **100**, 114115. http://dx.doi.org/10.1063/1.2369650

[16] Tsai, K.-C., Wu, W.-F., Chao, C.-G., Lee, J.-T. and Shen, S.-W. (2006) Improving Electrical Properties and Thermal Stability of (Ba,Sr)TiO_3 Thin Films on Cu(Mg) Bottom Electrodes. *Japan Journal of Applied Physics*, **45**, 5495-5500. http://dx.doi.org/10.1143/JJAP.45.5495

[17] Subramanyam, G., Ahamed, F. and Biggers, R. (2005) A SiMMIC Compatible Ferroelectric Varactor Shunt Switch for Microwave Applications. *IEEE Microwave and Wireless Components Letters*, **15**, 739-741. http://dx.doi.org/10.1109/LMWC.2005.858992

[18] Ahmed, M.A., Kamal, M., El Desouky, F.G., Girgis, E., Farag, I.S.A. and Batttisha, I.K. (2013) Synthesis and Characterization of Cobalt-Doped Nano-Structure Barium Strontium Titanate Prepared by Sol-Gel Process. *Journal of Applied Sciences Research*, **9**, 2432-2438.

[19] Culity, B.D. and Graham C.D. (2009) Introduction to Magnetic Materials. John Wiley, Sons, Inc., Hoboken, New Jersey.

[20] Guo, Z., Pan, L., Qiu, C.H., Zhao, X., Yang, L. and Rafique, M.Y. (2013) Structural and Multiferroic Properties of Fe-Doped $Ba_{0.5}Sr_{0.5}TiO_3$ Solids. *Journal of MMM*, **325**, 24-28.